MICHIGAN STATE
UNIVERSITY

National Superconducting Cyclotron Laboratory

ISOSPIN EFFECTS IN FRAGMENT PRODUCTION

To be published in "Isospin Physics and Heavy-Ion Collisions at Intermediate Energies," Ed. Bao An Li, Nova Science Publishers, Inc. (2001)

M.B. TSANG, W.A. FRIEDMAN, W.G. LYNCH

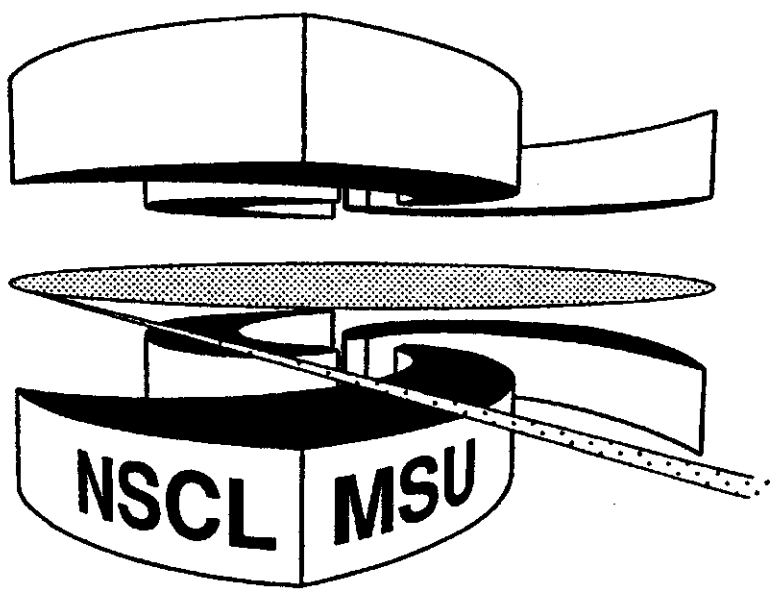

MSUCL-1179 **OCTOBER 2000**

Isospin Effects in Fragment Production

M. B. Tsang[1], W.A. Friedman[2], W.G. Lynch[1]

[1]*National Superconducting Cyclotron Laboratory and Department of Physics and Astronomy, Michigan State University, East Lansing, MI 48824, USA*
[2]*Department of Physics, University of Wisconsin, Madison, WI 53706*

Abstract

The dependence of isotope distribution on the overall isospin of the reaction system is investigated. General scaling curves are observed. The meaning of the observed isospoin effects is discussed for each of the different reaction.

In the past decade, substantial knowledge about the decay of excited systems formed in heavy ion collisions has been obtained from the measurement of the charge and energy of the emitted particles. Ideally information about these particles should include the identification of the isotopic composition, i.e., mass as well as charge. Reaction models, ranging in emphasis from statistical to dynamical, have been developed. These can account for many salient features, such as the charge and energy distributions of the elements produced in multifragmentation. However, precise experimental isotope distributions have been difficult to reproduce with theoretical models due to complications arising from the role of sequential decays [1-3]. Inclusions of nuclear spectral information into the calculations to simulate the effects of secondary decay has not been fully successful because the task is not only computationally difficult, but is also hampered by the lack of complete information about the resonances in many nuclei [3].

The importance of the isotopic degree of freedom, a) to obtain information about charge equilibration, b) to understand the behavior of the charge asymmetry features of the nuclear equation-of-state, and c) to provide strenuous tests for reaction models, has prompted the design of experiments with the specific capability of measuring isotope distributions [4,5]. Figure 1 shows the

measured differential multiplicities of Li, Be, B, C, N and O isotopes at $\theta_{CM}=90°$ for three systems, $^{112}Sn+^{112}Sn$ (open circles), $^{112}Sn+^{124}Sn$ (open diamonds [6]) and $^{124}Sn+^{124}Sn$ (closed circles) measured by the LASSA collaboration at E/A=50 MeV [5]. These data are selected for central collisions by a gate on charged particle multiplicity and are subjected to a gate on rapidity of $0.46 \le y/y_{beam} \le 0.65$. More detailed information about the experiment can be found in Ref. [5].

The x-axis, N-Z, corresponds to the neutron excess of the isotope. For $x=0$, these are symmetric isotopes with $N=Z$. The peaks of the distributions are

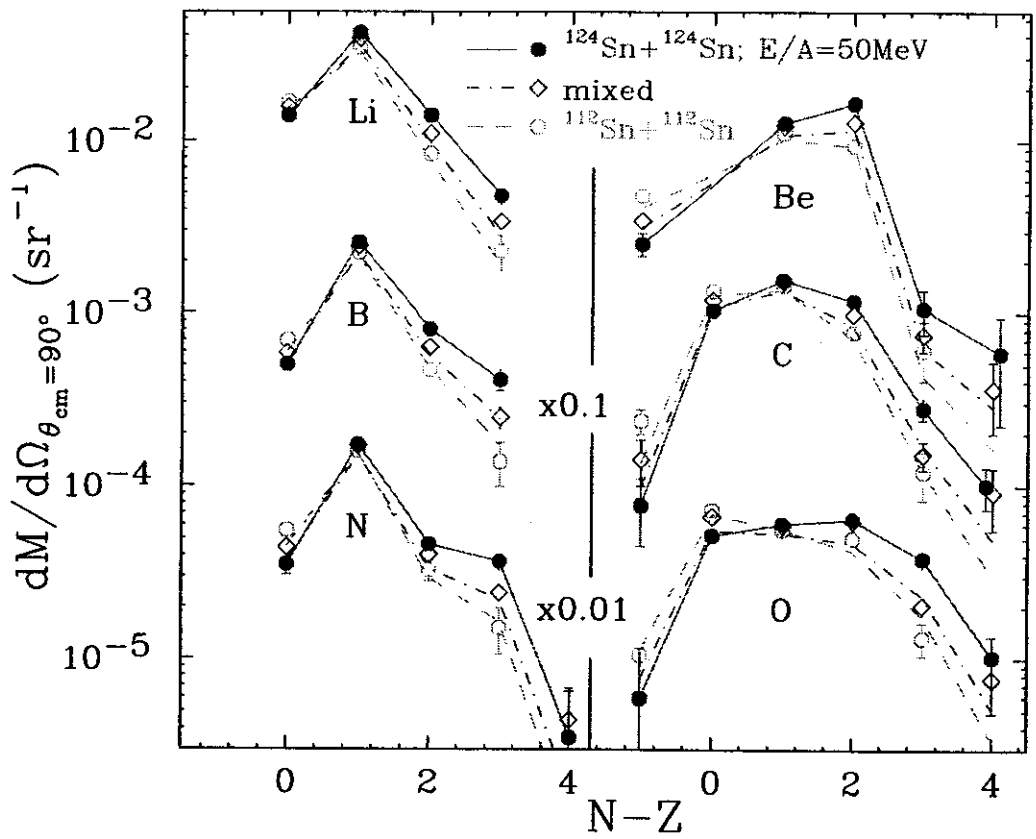

Figure 1: Differential multiplicities at $\theta_{CM}=90°$ for Li, Be, B, C, N and O isotopes as a function of neutron excess (N-Z) of the isotope. The solid points drawn by solid lines to guide the eyes are data for the $^{124}Sn+^{124}Sn$ system with $N/Z=1.48$. The open circles are data for the lightest system $^{112}Sn+^{112}Sn$ with $N/Z=1.24$. The open diamonds are the statistically averaged values from the two mixed systems, $^{124}Sn+^{112}Sn$ and $^{112}Sn+^{124}Sn$. The dashed and dotdashed lines are predictions from Eq. (4).

located around $N=Z+1$ isotopes. The yields of the boron, carbon isotopes are offset by a factor of 10 and the yields of the nitrogen and oxygen isotopes are offset by a factor of 100 in the figure. As expected, more neutron rich isotopes ($N-Z>0$) are produced by the neutron rich system, $^{124}Sn+^{124}Sn$, while the opposite is true for the proton-rich isotope yields. In general, the drop from the peak toward more proton-rich isotopes is steeper than the corresponding drop towards the neutron rich isotopes. The difference in isotope yields between the three different systems is not very large, less than a factor of two for the more abundant isotopes. The difference increases at the extremes of the isotope distributions. Thus larger differences may occur at more extreme values of the asymmetry but such data have not been obtained in this experiment.

Multifragmentation processes have been successfully described by statistical theory suggesting their cross sections are dominated by phase space. In this limit, one may obtain some guidance from the simple dependence of the population of isotopes predicted by the equilibrium limit of the Grand-Canonical Ensemble [7,8]. For this special case the yield of isotopes is governed by two nucleon chemical potentials, μ_n, μ_p and the temperature T plus the individual binding energies of the various isotopes $B(N,Z)$.

$$Y(N,Z)=F(N,Z,T)\,e^{B(N,Z)/T}\,e^{(N\mu_n+Z\mu_p)/T} \qquad (1)$$

In the Grand-Canonical limit, the chemical potentials are related to the nucleon density, $\rho_n \propto e^{\mu_n/T}$ and $\rho_p \propto e^{\mu_p/T}$. The factor $F(N,Z,T)$ includes information about the change of the yield arising from secondary feeding and the temperature of the isotope considered. It reflects the sequential feeding contribution from the particle stable states of the same nucleus or from the particle decay of heavier unbound nuclei.

From charge symmetry, mirror nuclei with $|N-Z|=1$ have similar internal partition functions. Therefore secondary feeding from the particle stable states in Eq. (1) are similar for mirror nuclei. If the sequential decay effects from unbound

particle states and the influence of the Coulomb interaction with remaining system are small, the dependence of isobaric yield ratios on the binding energy difference should be exponential, i.e.

$$Y(N,Z)/Y(Z,N) \propto exp[(\mu_p-\mu_n)/T] \propto (\rho_n/\rho_p)\, e^{\Delta B/T} \qquad (2)$$

Figure 2 shows the isobaric yield ratios of three pairs of mirror nuclei, (t, ^{3}He), (^{7}Li, ^{7}Be) and (^{11}B, ^{11}C), as a function of the binding energy difference, ΔB for two reactions, ^{112}Sn+^{112}Sn (open points) and ^{124}Sn+^{124}Sn (solid points) at E/A=50 MeV. Equation (2) suggests that the dependence of the isobaric yield ratios on the binding energy difference should be exponential. In fact, the experimental

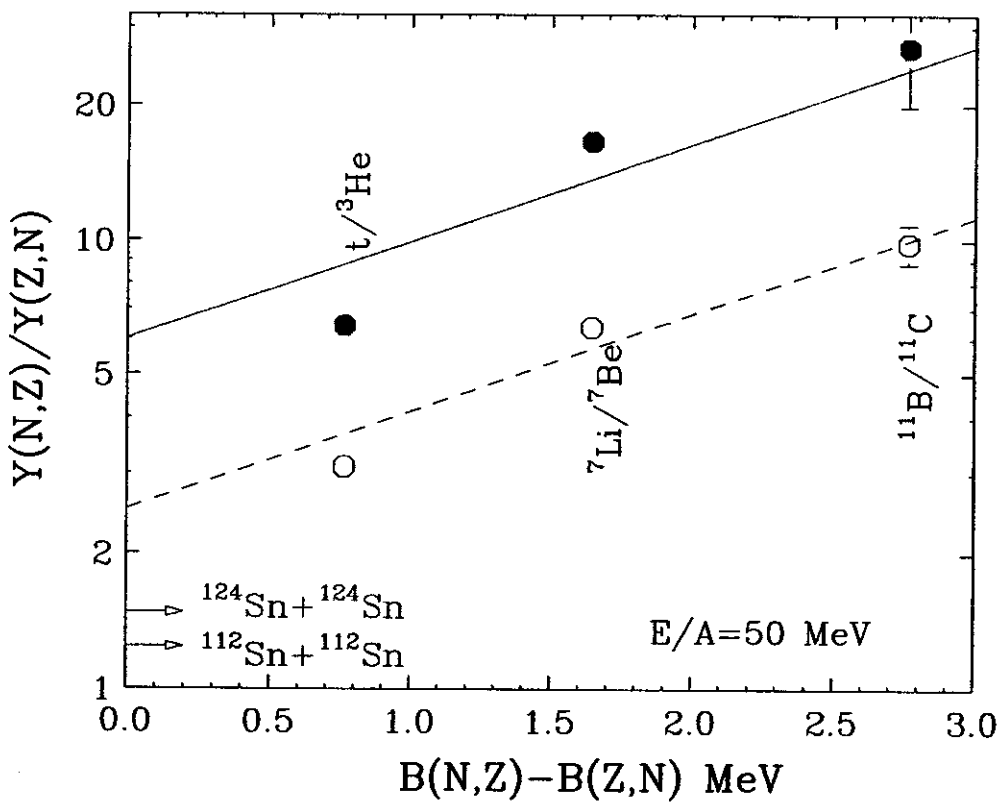

Figure 2: Isobar ratios for three pairs of mirror nuclei obtained from the ^{112}Sn+^{112}Sn (open circles) and ^{124}Sn+^{124}Sn (solid points) reactions. The lines are best-fit parameterizations of Eq. (2)

data fluctuate around such a relationship. Extrapolation to $\Delta B=0$ using the best fit lines (dashed and solid lines) suggests values for ρ_n / ρ_p of 2.5 for the $^{112}Sn+^{112}Sn$ system (bottom line) and 5.5 for the $^{124}Sn+^{124}Sn$ system (top line). Both of these numbers are larger than the initial N/Z values of the two systems, 1.24 and 1.48, (marked by the two arrows in the figure) for $^{112}Sn+^{112}Sn$ and $^{124}Sn+^{124}Sn$, respectively. Statistical interpretations of the mirror nuclei yield ratios suggest a change of 2.5 in the N/Z ratio, which is clearly larger than 20% change in the total N/Z.

The mirror nuclei ratios shown in Figure 2 do not follow Eq. (2) strictly, partly because the difference in the Coulomb interaction is neglected but also because, the secondary feedings from particle unstable states are large. Statistical calculations suggest that these ratios can be reduced by as much as a factor of two due to sequential decays [9].

To search for experimental observables that are minimally affected by secondary decays, we note that the corrections to the primary yields due to secondary decays appear to be similar from reaction to reaction over a wide range of bombarding energies [10]. Taking this similarity into account, the isotope yields of two different systems with similar incident (excitation) energies but different isospins can be combined to construct ratios of the form,

$$R_{21}(N,Z) = \frac{Y_2(N,Z)}{Y_1(N,Z)}. \qquad (3)$$

(Throughout this article, we have chosen the system in the numerator to be more neutron-rich than the one in the denominator.) Statistical calculations predict R_{21} to be insensitive to sequential decay effects. R_{21} constructed from primary yields appears to be quite close to the values of R_{21} extracted from the secondary yields [5, 9].

If the system is in equilibrium and $F_1(N,Z,T) = F_2(N,Z,T)$, one might anticipate that $R_{21}(N,Z)$ is governed by only three parameters:

$$R_{21}(N,Z) \sim Ce^{N\alpha+Z\beta} \qquad (4)$$

where $\alpha=\Delta\mu_n/T$ and $\beta=\Delta\mu_p/T$ reflect the differences between the neutron and proton chemical potentials for the two reactions and C is an overall normalization constant. The N and Z dependence becomes most apparent if, for each element Z, R_{21} is plotted versus N for all isotopes on a semi-log plot. The resulting slopes would then be α for each Z. Similarly, plotting R_{21} against Z for all isotones would provide a common slope β for each N. This is demonstrated in Figure 3 where the isotope yield ratios from the central collisions of $^{124}Sn+^{124}Sn$

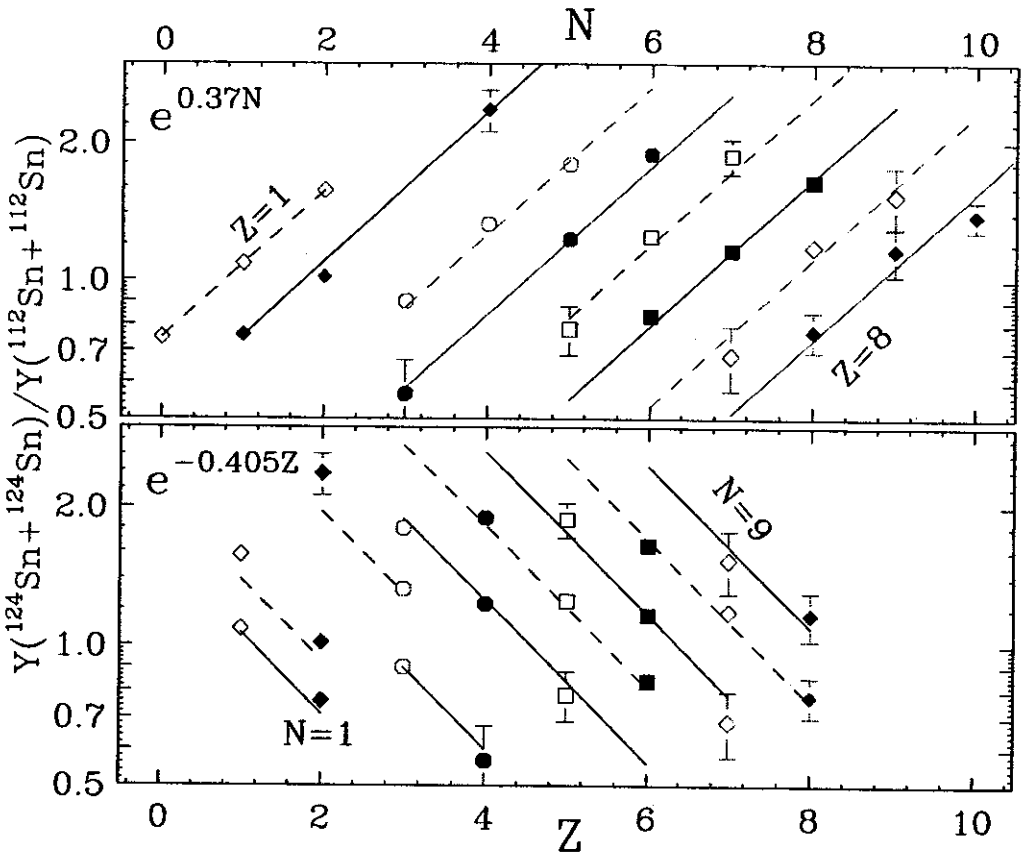

Figure 3: R_{21} for $^{124}Sn+^{124}Sn$ and $^{112}Sn+^{112}Sn$ systems, as a function of N (isotope data, upper panel) and as a function of Z (isotone data, lower panel). Solid and dashed lines are best fits to the data.

and $^{112}Sn+^{112}Sn$ are plotted as a function of N (upper panel) and as a function of Z (lower panel) for 24 isotopes spanning from Z =1 to Z=8 elements. The excellent agreement between data and Eq. (4) can be seen more clearly by comparing the experimental ratios with the best fits of straight lines with α=0.36 and β=-0.41.

In the Grand Canonical Ensemble limit of dilute non-interacting gas, α and β are related to the relative nucleon density, $\hat{\rho}_n = \rho_n^2 / \rho_n^1 = e^{\alpha}$ and $\hat{\rho}_p = \rho_p^2 / \rho_p^1 = e^{\beta}$ [5]. The resulting values, of $\hat{\rho}_n$ and $\hat{\rho}_p$, extracted from isotope ratios for the three systems: $^{112}Sn+^{112}Sn$, $^{124}Sn+^{112}Sn$, $^{124}Sn+^{124}Sn$ are shown in Fig. 4 as a function of the N/Z ratio of the composite system, $(N/Z)_o$. The trend of the total neutron and

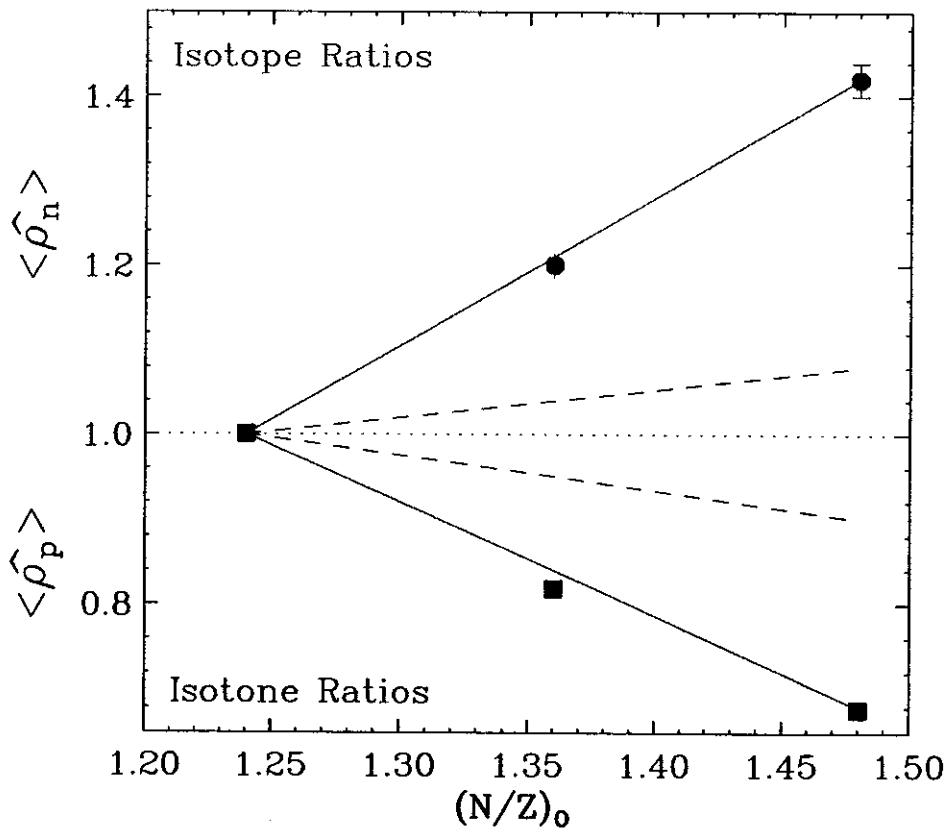

Figure 4: The relative free neutron $\hat{\rho}_n = e^{\alpha}$ and free proton density $\hat{\rho}_p = e^{\beta}$ as a function of $(N/Z)_o$. The solid lines are best fit through the data. The dashed lines are the expected n-enrichment and p-depletion with the increase of isospin of the initial systems.

proton density, assuming the same total matter density for the two systems, is given by the dashed lines in Fig. 4. The experimental data suggest that as $(N/Z)_o$ increases, the system responds by making the asymmetry of the gas (given by the solid lines) much greater than the asymmetry of the total system (given by the dashed lines). The extracted $\hat{\rho}_n / \hat{\rho}_p \approx 2$ at $(N/Z)_o=1.48$ is roughly consistent with the mirror nuclei ratios obtained in Figure 2 for the $^{124}Sn+^{124}Sn$ and $^{112}Sn+^{112}Sn$ systems.

If the equilibrium interpretation of these data is correct, the nucleon density extracted from isotope, isotone and isobar ratios is more enriched in neutrons than the liquid phase represented by bound nuclei, consistent with the predicted partial fractionation of nucleon components in the liquid gas phase transition [11, 12]. The neutron enrichment is much more enhanced in the collisions of neutron-rich systems as compared to collisions of neutron-deficient system.

A more compact way of plotting the data in Figure 3 is to construct the scaling factor $S(\beta)=R_{21}(-\beta Z)$. With the best fit value of β, all isotopes would lie on a single line if $S(\beta)$ is plotted versus N on a semi-log plot. This trend is referred as "scaling". The scaling behavior of the data shown in Figure 3 is illustrated in Figure 5. The data are plotted next to the label "multifragmentation". Isotopes from Lithium to Oxygen lie on a line. The hydrogen and helium isotopes lie slightly above the line even though each element still has the same slope. This small deviation may result if light particles such as hydrogen and helium are produced by different mechanisms, for example pre-equilibrium emission.

This systematics, suggested by the grand canonical expression, appears to be more generally respected than one might expect. For example, evaporation process displays similar scaling behavior. Figure 5 shows the scaling factor $S(\beta)$ determined for isotopes detected at backward angles ($\theta_{lab}=154°$) in the reactions $^4He+^{116}Sn$ and $^4He+^{124}Sn$ at an incident energy of 200 MeV [13]. These data are

plotted next to the label "evaporation". The dashed line drawn through the data is a best fit to this data using Eq. 4.

For the low energy collisions of ^{16}O with two targets, ^{232}Th and ^{197}Au, at E/A=8.6 MeV [14], we have plotted the scaling factor $S(\beta)$ obtained for strongly damped reactions. At such energies, just above the Coulomb barrier, the isotopes originate from the breakup of di-nuclear systems formed by the transfer of

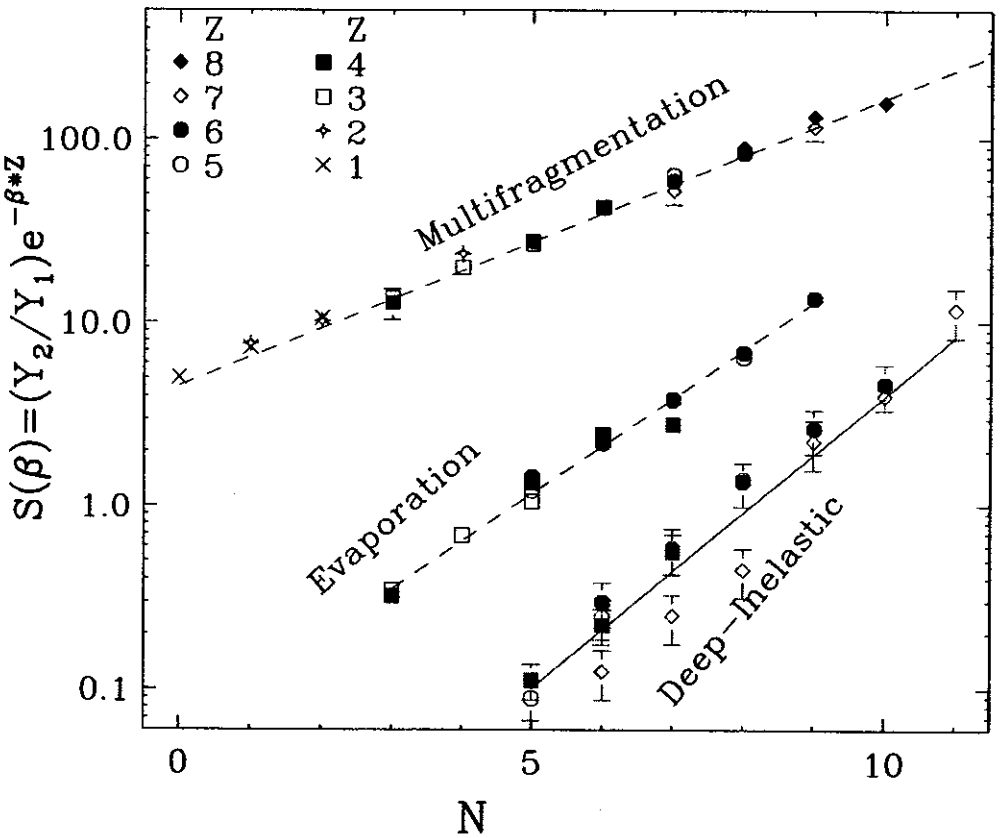

Figure 5: The scaled isotopic ratio, $S(\beta)$ is plotted as a function of N using the best fit value of β obtained from fitting isotopes with $Z \geq 3$. The data points plotted next to the label "multifragmentation" denote $S(\beta)$ extracted from multifragmentation events in proton density, assuming the same total matter density for the two systems, iscentral $^{112}Sn+^{112}Sn$ and $^{124}Sn+^{124}Sn$ collisions [5]. The scaling behavior for evaporation process is illustrated by the reactions $^{4}He+^{116}Sn$ and $^{4}He+^{124}Sn$ [13] plotted next to the label "evaporation". Systematics of the strongly damped binary collisions is represented by the data of ^{16}O induced reactions on two targets ^{232}Th and ^{197}Au [14] plotted next to the label "deep-inelastic".

energy and mass between projectile and target. These data are plotted next to the label "deep inelastic" in Figure 5 and the best fit line is also drawn through the data.

Figure 5 suggests that the scaling behavior appears to be a surprisingly robust feature over a range of data from deep-inelastic heavy ion reactions at lowest energies, through evaporation reactions induced by light and heavy ion projectiles, to high energy heavy ion reactions characterized by the copious production of intermediate mass fragments (IMFs) and multifragmentation. For evaporation and deeply inelastic processes, the grand-canonical ensemble approach of Eq. (1) has little relevance. Why the scaling phenomenon occurs in these cases is discussed below.

At large scattering angles of deeply inelastic reactions, it is frequently assumed that equilibrium is established in the binary system and the two fragments come to a common temperature [14]. Empirically it is observed that the isotope yields are correlated with the Q-value for the mass transfer, known as the "Q_{gg} -systematics". The observation of Q_{gg}-systematics in the $^{16}O + ^{232}Th$ and $^{16}O + ^{197}Au$ reactions, implies that the yield ratios can be expressed in terms of the difference between the binding energies of the two binary reaction partners.

$$R_{21} \propto exp\,[(BE(N_2\text{-}N,Z_2\text{-}Z)\text{-}BE(N_1\text{-}N,Z_1\text{-}Z))/T],$$

$$\approx exp\,[(-\Delta S_n \cdot N - \Delta S_p \cdot Z)/T] \qquad (5)$$

where Z_i and N_i are the total proton and neutron number of reaction i. $BE(N,Z)$ is the binding energy of a nucleus with neutron number N and proton number Z. Expanding the binding energies in Eq. (5) in Taylor series, one can obtain an approximation similar to Eq. (4) that is first order in N and Z. In this expression, the role of the chemical potential difference in Eq. (4), is played by the difference of the average neutron and proton separation energies, ΔS_n and ΔS_p.

The underlying origin of the scaling behavior observed in evaporation processes turns out to be similar to that found in the case of deep inelastic

scattering. Using the formalism proposed by Friedman and Lynch [15] and performing another Taylor expansion, the relative isotope ratio can be written as

$$R_{21} \propto exp\,[\{(-\Delta S_n + \Delta f_n^*)\cdot N + (-\Delta S_p + \Delta f_p^* + e\Delta\Phi(Z_i - Z))\cdot Z\}/T] \qquad (6)$$

where the terms $f_n^*(f_p^*)$ represent the excitation energy contribution to the free energy per neutron (proton) and Φ is the electrostatic potential at the surface of the nuclei. More detailed discussions of Eq. (5) and (6) can be found in Ref. [16]. While first order terms in the Taylor expansion dominate for small A<12, it can be expected that the scaling behavior will breakdown at high Z and N values.

Equation (6) is also consistent with multifragmentation description that follows the Expanding Emitting Source (EES) model [17]. In that model the evaporation considerations discussed above are coupled to an expansion process which reduces the density of the emitting system. The density dependence of the various terms in the exponent in Eq. (6) becomes important. If the expansion were to be isentropic, then the temperature would vary as $\rho^{2/3}$. Likewise, the Fermi energy would also be anticipated to vary with the density $\rho^{2/3}$. Thus, for a Fermi gas, $\Delta f/T$ would remain constant even with reducing density. As seen in the evaporation process, the value of ΔS_n and ΔS_p are strongly governed by the symmetry term contributions to the masses. If the system is expanding, dependence of the symmetry term on density will be important. Model calculations suggest that the low energy density dependence of the symmetry energy may vary with the density to the 2/3 power. In that case the ratio of symmetry energy to temperature for an isentropic expansion may remain constant with reducing density. Thus for isentropic expansion and the specific assumptions for the density dependences we have outlined, the EES rates will provide a constant ratio over the expansion process, so that R_{21} can be determined by the initial conditions. On the other hand, EES calculations, predict that the emission of IMFs occurs strongly at a stage of large expansion, with densities on the order of 1/3 of normal density and temperatures on the order of

5 MeV. Thus R_{21} can, more generally, be determined by the particular values of the symmetry energy under the conditions of reduced density without any assumption for a specific density dependence. Consequently, a measurement of the observable R_{21} can be used to probe the density dependence of the symmetry energy. This is one of the anticipated benefits of future studies of the R_{21} parameter.

The EES predictions also suggest that the *N/Z* of the emitting system may be modified by early emission of light fragments, so detailed comparison between data and freeze-out models requires an estimate of this change. At present, an analogous procedure is attempted to adjust both energy loss and mass loss in the early stages of the reaction leading to the freeze-out. Additional care will be required in estimating the isospin of the freeze-out source.

Figure 5 suggests that the scaling behavior is a general property of heavy ion reactions where some form of equilibrium is established. If two systems are employed in constructing values of R_{21}, the observation of the systematic trends does not imply that both reacting systems proceed with the same reaction mechanism. Additional information is needed to elucidate details of the underlying reaction mechanism [16].

Since most data obtained in the past do not have a large range of well measured isotope yields, one can investigate the criterions for scaling behavior using the double ratio which is related to the slope of the logarithm of the scaling function,

$$\mathrm{R4} = \frac{Y_2(N_i+1,Z_i)}{Y_2(N_i,Z_i)} \Big/ \frac{Y_1(N_i+1,Z_i)}{Y_1(N_i,Z_i)} = e^{\alpha} \qquad (7)$$

This formula relates α to specific isotope double ratios; a similar formula has been obtained by ref. [5], which relates corresponding isotone ratios to β. As shown in ref. [5], use of Eq. (7) is equivalent to fitting the systematics shown in Fig. 3. R4 has the advantage that values for α or β can be obtained very easily

from a sparse data set. To illustrate its functionality, we show experimental values for *R4* in the lower panel of Fig. 6 which were obtained from ref. [13,18,19] for four systems $^{4}He+^{116}Sn$ at 200 MeV, $^{4}He+^{124}Sn$ at 200 MeV, *p+Ag* at 480 MeV and *p+U* at 5.5 GeV at backward angles, $\theta_{lab} > 150°$. While the incident energies of these systems are different, values for the temperature extracted from isotopic thermometry measurements are statistically consistent with an average value of about 2.7 MeV [20]. (At such low temperatures, the corrections to the isotopic thermometer for secondary decay should be small [2].) Thus, one may be justified with comparing the isotopic yields via an R_{21} or *R4* ratio and analyzing the result via an evaporation expression such as that given in Eq. (6). A linear

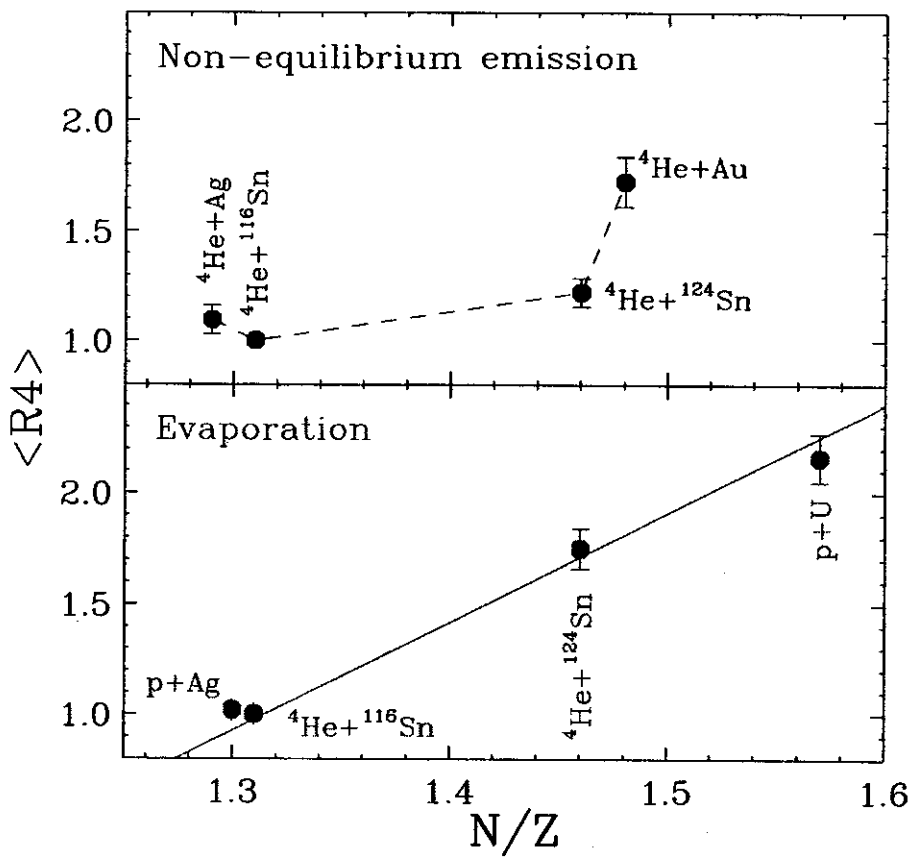

Figure 6: The *N/Z* dependence of *R4* for isotopes produced in evaporation reactions at backward angles (bottom panel) [13,18,19] and for isotopes measured in non-equilibirium emissions at forward angles (top panel) [13, 21].

dependence of the resulting *R4* values upon *N/Z* is expected (see Fig. 4), and its confirmation (solid line drawn to guide the eye) in the lower panel of Fig. 6 supports the expectation that all four systems are at a similar temperature. The slope, which reflects the lower temperature *(T~2.7 MeV)* of the evaporation systems is steeper than that shown in Figure 4 for the *Sn+Sn* systems, which have a higher temperature *(T~4 MeV).*

The upper panel shows a similar comparison involving the isotopic yields emitted to forward angles where preequilibrium emission is important [13]. Here, *R4* values for $^{4}He+^{116}Sn$ and $^{4}He+^{124}Sn$ reactions at 200 MeV and $\theta_{lab}=12^{\circ}$ [13] as well as $^{3}He+Ag$ and $^{3}He+Au$ at 200 MeV and $\theta_{lab}=12^{\circ}$ [21] are plotted. As in the case with the backward angle measurements, we note that the isotopic temperatures in these reactions have roughly the same value [20], about 4.3 MeV. Contrary to the data plotted in the lower panel, no clear systematic trends emerge. Very likely such comparisons are complicated by the fact that the yields used in *R4* are strongly angle dependent reflecting the strong forward focusing of the preequilibrium component of the spectrum. Whether or not systematic trends would emerge if the isotopic yields for preequilibrium emission were extracted instead by a moving source decomposition of equilibrium and preequilibrium sources is unclear. In any case, the observation of systematic trends in *R4* is not guaranteed; some care to make sure that the emission mechanism is thermal and that one knows how to correct the yields for the kinematic focusing of the reaction mechanism appears to be required. Similar problems were encountered in extracting $<R4>$ for 660 MeV proton induced reactions on $^{10,11}B$, $^{58,64}Ni$, $^{112,124}Sn$, $^{150,154}Sm$ at $\theta_{lab}=90^{\circ}$ [22] and 1 GeV proton induced reactions on *Ti*, $^{58,64}Ni$, $^{112,124}Sn$ at $\theta_{lab}=60^{\circ}$[23].

In summary, we have examined the isotope yields produced in heavy ions collisions over a wide range of energy and projectile, target combinations. In situations where equilibrium is established to the extent that a temperature may be defined, a general scaling is observed. This allows a transparent

characterization of the dependence of isotope distributions on the overall isospin of the system. This scaling applies to a broad range of statistical production mechanisms including evaporation, strongly damped binary collision, and multifragmentation. We have shown how this systematics can be explained by theories frequently applied to such processes. In the case of multifragmentation, within the grand canonical ensemble limit, the scaling behavior can be interpreted as isospin fractionation. The nucleon density extracted from the gas phase using isotope, isotone and isobar ratios of four Sn+Sn systems suggest that the gas phase is more enriched in neutrons than the liquid phase represented by bound nuclei, consistent with the predicted partial fractionation of nucleon components in the liquid gas phase transition. The observed effects are significantly enhanced in neutron-rich systems relative to neutron-deficient systems.

This work was supported by the National Science Foundation under Grant Nos. PHY-95-28844 and PHY-96-05140.

References:

[1] T.K. Nayak, T. Murakami, W.G. Lynch, K. Swartz, D.J. Fields, C.K. Gelbke, Y.D. Kim, J. Pochodzalla, M.B. Tsang, H.M. Xu, F. Zhu, K. Kwiatkowski; Phys. Rev. C**45**, 132 (1992).

[2] H. Xi, W.G. Lynch, M.B. Tsang, W.A. Friedman, D. Durand; Phys. Rev C**59**, 1567 (1999).

[3] S.R. Souza, W.P. Tan, R. Donangelo, C.K. Gelbke, W.G. Lynch, M.B. Tsang; Phys. Rev. C (in press).

[4] S.J. Yennello; see article in the same Volume.

[5] H.S. Xu, M.B. Tsang, T.X. Liu, X.D. Liu, W.G. Lynch, W.P. Tan and G. Verde, L. Beaulieu, B. Davin, Y. Larochelle, T. Lefort, R.T. de Souza, R. Yanez, V.E. Viola, R.J. Charity, L.G. Sobotka; Phys. Rev. Lett. **85**, 716 (2000)

[6] The mixed system data shown in Fig. 1 and 4 are the statistical average of two systems $^{124}Sn+^{112}Sn$ and $^{112}Sn+^{124}Sn$.

[7] J. Randrup, S.E. Koonin; Nucl. Phys. **A356**, 223(1981).

[8] S. Albergo et al.; Nuovo Cimento **A89**, 1 (1985).

[9] W.P. Tan, private communication.

[10] M.B. Tsang, W. G. Lynch, H. Xi, W.A. Friedman; Phys. Rev. Lett. **78**, 3836 (1997).

[1] Horst Muller, Brian D. Serot; Phys. Rev. **C52**, 2072 (1995).

[12] F. Gulminelli, Ph. Chomaz, Phys. Rev. Lett. **82**,1402 (1999). Also see article by Chomaz in the present volume.

[13] J. Brzychczyk, D. S. Bracken, K. Kwiatkowski, K. B. Morley, E. Renshaw Foxford, V. E.Viola, Phys. Rev. **C47**, 1553 (1993).

[14] V.V. Volkov, Phys. Rep. **44**, 93, (1978).

[15] W. Friedman and W. Lynch, Phys. Rev. C **28**, 950 (1983).

[16] M. B. Tsang, W.A. Friedman, C.K. Gelbke, W.G. Lynch, G. Verde, H. Xu, NSCL_1165 (July, 2000) and to be published.

[17] W.A. Friedman, Phys. Rev. Lett. **60**, 2125 (1988); and Phys. Rev. **C42**, 667 (1990).

[18] Ray E.L. Green, Ralph G. Korteling, K. Peter Jackson, Phys. Rev. C **29**, 1806 (1984).

[19] A.M. Poskanzer, Gilbert W. Butler, and Earl K. Hyde PRC 3, 882 (1973)

[20] V. E. Viola, K. Kwiatkowski, W. A. Friedman, Phys. Rev. C **59**, 2660 (1999)

[21] J. Zhang, K. Kwiatkowski, D. Bonser, M. Fatyga, S.D. Coon, K. Stith, V.E. Viola, L.W. Woo and S.J. Yennello, Phys. Rev. C **56**, 1918 (1997).

[22] V.I. Bogatin, V.F. Litvin, O.V. Lozhkin, N.Z. Perfilov and Yu. P. Yakovlev, Nucl. Phys. **A260**, 446 (1976).

[23] E.N. Volnin, G.M. Amalsky, D.M. Seleverstov, N.N. Smirnov, A.A. Vorobyov and Yu. P. Yakovlev, Phys. Lett. **55B** 409 (1975)